

One possible explanation for the Balmer and Lyman line shifts in quasars

Dangbo Liu¹, Jianrong Shi², Junhan You¹

¹*Center for Astronomy and Astrophysics, Department of Physics and Astronomy, and Shanghai Key Lab for Particle Physics and Cosmology, Shanghai Jiao Tong University, 800 Dongchuan Road, 200240, Shanghai, China*

²*Key Laboratory of Optical Astronomy, National Astronomical Observatories, Chinese Academy of Sciences, 100012, Beijing, China*

ABSTRACT

Internal line shifts in quasars spectra have played a more prominent role in our understanding of quasar structure and dynamics. The observed different redshift among broad hydrogen lines is still an amazing puzzle in the study of quasars. We have argued that the broad hydrogen lines, as well as the low-ionization lines in quasars, are significantly contributed by the Cerenkov quasi-line emission of the fast electrons in the dense clouds/filaments/sheets ($N_{\text{H}} \geq 10^{14} \text{ cm}^{-3}$); whereas this line-like radiation mechanism is invalid for producing the high ionization lines. In order to account for redshift difference, the Cerenkov line-like radiation mechanism could provide a plausible resolution: it is the ‘Cerenkov line redshift’, which is different from line to line, causes the peculiar redshift-differences among Ly α , H α and H β lines. The different redshifts among different broad hydrogen lines could stand for an evidence to quantitatively support that the observed broad hydrogen lines should be blended by both the real line emission and the Cerenkov quasi-line emission. The good fitting to the observed redshifts of quasars confirms the existence of Cerenkov component in the broad hydrogen lines, which indicates that, in the blended Ly α line, the line-intensity of the Cerenkov component approximately equals that of the accompanying ‘normal line’ (an approximate equipartition of intensity between the two components in the broad Ly α line). This result illustrates the importance of the Cerenkov component in the broad lines of quasars, which can be further confirmed by future observations.

Subject headings: line: formation — method: analytical — quasars: emission lines — radiation mechanism: non-thermal

1. Introduction

The emission lines are used to probe to the structure and dynamics of the radiation region around the massive black holes in quasars. In the early 1970s, peculiar Balmer line profiles had attracted people’s attentions, and all lines in a quasar do not produce the same redshift, howbeit the redshift difference between emission lines had not been systematically studied in quasars since the 1980s, even if some broad line shifts with respect to narrow lines had been reported in quasars (Osterbrock 1979). The different values for low-ionization lines (LILs) to be red-shifted relative to high-ionization lines (HILs) has been well noted (Gaskell 1982; Wilkes 1986; Espey et al. 1989; Corbin 1990; Carswell et al. 1991; Sulentic et al. 1995; McIntosh et al. 1999). Recently, Vanden Berk et al. (2001) compiled a sample of over 2200 quasars from the SDSS data and created a variety of composite quasar spectra. The existence of slight redshifts of LILs with respect to HILs is confirmed. The most peculiar result in their composite spectra is suggesting a redshift difference between the $H\alpha$ and $H\beta$ lines, $\Delta Z = Z_\alpha - Z_\beta \approx 10^{-4}$ (see Table 4 of Vanden Berk et al. 2001). Observations show this trend of $Z_\alpha > Z_\beta$ seems universal (see e.g., Table 4 in Vanden Berk et al. 2001, also see, Tables 1 and 2 in Cheng et al. 1990 and Table 2 in Nishihara et al. 1997). Over the past decades, some physical and dynamical interpretations of line shifts have been developed in the study of quasars such as atomic physics, scattering processes, gravitational redshift, Doppler effect, etc. (Halenka et al. 2015; Korista 1992; Halpern & Eracleous 2000; Ji et al. 2012; Davidson & Netzer 1979; Smith et al. 2005; Laor 2006; Gaskell & Goosmann 2013; Netzer 1977; Koratkar & Gaskell 1991; Peterson & Wandel 1999; Shadmehri 2015), however, just as described in the review paper by Sulentic et al. (2016), the systematical redshift differences between emission lines in quasars have not been fully clarified, and the structure and dynamics of the regions emitting the low-ionization lines (LILs) are not fully understood. The physical models associated dynamical processes in quasars need to be further developed.

In our recent paper (Liu et al. 2014), we claimed that the Cerenkov line-like radiation, created by the fast electrons in the dense clouds/filaments/sheets with high densities $N_H \geq 10^{14} \text{ cm}^{-3}$, has a significant contribution to the broad hydrogen lines and low-ionization lines of quasars. Therefore the observed broad hydrogen line or low-ionization lines(LILs) should be a ‘blended line’ with two components: the ‘normal line’, exactly at $\lambda = \lambda_{lu}$, produced by the bound-bound transition $u \rightarrow l$ in atoms/ions, and the ‘Cerenkov quasi-line’. Actually, the latter is not a real emission line, instead, it is a narrow continuum near the intrinsic wavelength λ_{lu} of a hydrogen line, $\lambda \gtrsim \lambda_{lu}$, hence the name ‘Cerenkov line-like radiation’, or simply , ‘Cerenkov quasi-line’. Besides, we mentioned that the high ionization lines(HILs) (e.g., C III, C IV, N V, etc.) are pure ‘normal lines’, because the Cerenkov radiation disappears in a fully ionized dense hydrogen plasma, where all high-valence ions reside (e.g., C^{++} , C^{3+} , N^{4+} , etc.). In this region, the Cerenkov mechanism does not work due to the ‘effect

of plasma oscillation’, rendering the refractive index of plasma $n < 1$ (see also, Chen et al. 2005). Therefore, supposing that the HILs are pure normal lines and the LILs are blended lines with the two components of normal line and Cerenkov quasi-line, this will be a plausible possibility to result in the difference between LILs and HILs, represented by Mg II (2800 Å) and C IV (1549 Å) respectively (Gaskell 1982) (detailed discussion in Section 5). We should indicate that the mechanism has been verified by laboratory experiments (Xu et al. 1988; Yang et al. 1988; Catravas et al. 2001).

In this paper, we provide an observation evidence, quantitatively supporting the above conclusions. We have mentioned that (see, You et al. 1984, 1986, 2000; Chen et al. 2005), one of the interesting properties of the Cerenkov quasi-line is that, it does not exactly locate at $\lambda = \lambda_{lu}$, but is slightly redshifted, called as the ‘Cerenkov line redshift’, which has a different amount of redshift from line to line (You et al. 1984, 1986, 2000). We try to find evidences in observations to confirm the reality of this newly recognized redshift. Our effort is successful. In Section 4 of this paper, by using this new redshift effect and based on the blend models, we calculate the redshifts of different hydrogen lines to compare with the observations. The good fitting very favors the proposition of the ‘blend line’.

Table 1 of this paper (in Section 3) shows the averaged additional redshifts, $\Delta Z_{Ly\alpha}^{obs}$, $\Delta Z_{H\alpha}^{obs}$, $\Delta Z_{H\beta}^{obs}$, of $\sim 2,200$ quasars, relative to the observed narrow line [O III] 5007 Å (see the first line in Table 1, Section 3. Data are taken from Table 4 in Vanden Berk et al. (2001), where the redshift is in unit of velocity. Note that, the redshift data of another strong hydrogen line Ly β is absent in their Table 4; hence absent in our Table 1. But we still list the expected redshift of Ly β line in the third line in Table 1 for future detections in observations). The observed redshifts of hydrogen lines Ly α , H α and H β in the first line of Table 1 are really different from each other. As mentioned above, the Cerenkov component in the proposed ‘blended line’ has an additional ‘Cerenkov line redshift’ with different amount for different lines. It is likely that the observed redshift-differences of different hydrogen lines could arise from this additional redshift, rather than from a velocity-origin, adopted in prevailing explanations.

Historically, it has been well known that, the low-ionization lines(LILs) and the hydrogen lines of quasars have a systemic redshift relative to the high-ionization lines(HILs) (Gaskell 1982; Wilkes 1986; Corbin 1990, 1991; Espey et al. 1989; Carswell et al. 1991; Sulentic et al. 1995; McIntosh et al. 1999). A large sample of over 2,200 quasars from the Sloan Digital Sky Survey (SDSS) database are compiled and a variety of composite quasar spectra are obtained by Vanden Berk et al. (2001). They confirmed the existence of the slight redshifts of LILs, as well as the slight blueshifts of HILs, with respect to the narrow [O III] 5007 Å beyond all doubts. According to the current explanation, both the redshifts of LILs and the

blueshifts of HILs are attributed to the stratified structure of the broad line region (BLR) of quasars, with different radial velocities of different ionization regions (inflow and outflow). From the stratification models, it is inferred that there would be a correlation between the velocity shifts and the ionization potentials of spectral lines. This correlation is also confirmed by using the same composite quasar spectra (see Table 4 in Vanden Berk et al. 2001). However, an issue arises: why the velocity-shifts are so different among the broad hydrogen lines, for which the ionization potential is the same, $I_{\text{H}} = 13.6$ eV (see e.g., Table 4 in Vanden Berk et al. 2001, also see, Tables 1 and 2 in Cheng et al. 1990 and Table 2 in Nishihara et al. 1997). It was suggested that, the hydrogen line stratification may occur due to the different radiation transfer effects for different lines (e.g., Osterbrock & Ferland 2006; Bentz et al. 2010). The density gradient in BLR with distance would cause the stratification of different hydrogen lines, leading to the different velocity-shifts. This may be true, and deserves to give a further detailed analysis to confirm this viewpoint. But until now no quantitative fitting to the observed redshift-differences of hydrogen lines has been developed by this way. This situation promotes us to make an attempt to find alternative solutions for this puzzle.

This paper is arranged as follows. In Section 2, we describe the blend model for the broad lines of quasars. In Section 3, we first give the theoretical redshifts of the pure Cerenkov Ly α , Ly β , H α and H β lines, for preparing the subsequent calculation of the additional redshifts of the blended lines. The detailed model calculations of the redshifts of the blended hydrogen lines are presented in Section 4. Finally, conclusions and discussions are given in Section 5.

2. Blend model for the broad lines — Coexistence of two kinds of clouds/filaments with high and low densities in BLR

We first give a clearer description for the blend model of the broad lines of quasars, than in our recent paper (Liu et al. 2014). We have mentioned that, the coexistence and blend of two kinds of emission lines need a coexistence of two kinds of clouds/filaments with higher and lower densities in the BLR. The clouds/filaments with ‘standard’ densities $N_{\text{H}} \sim 10^9 - 10^{11} \text{ cm}^{-3}$ (Davidson & Netzer 1979), illuminated by the central UV and X-ray continuum, are responsible to the normal line emission, but they have little contribution to the Cerenkov lines (see Figure 1 in Liu et al. (2014)). On the other hand, in the very dense clouds/filaments with $N_{\text{H}} \sim 10^{14} - 10^{18} \text{ cm}^{-3}$, the Cerenkov line-like radiation occurs and becomes more prominent for higher densities; whereas the normal lines totally disappear because of the thermalization in the dense gas (when $N_{\text{H}} > 10^{13} \text{ cm}^{-3}$, see Rees et al. (1989)). In brief, the normal lines and the Cerenkov quasi-lines, respectively, arise from the ‘standard’

and the dense clouds/filaments in the BLR (intermediate densities of $10^{11} \text{ cm}^{-3} < N_{\text{H}} < 10^{14} \text{ cm}^{-3}$ are also possible—it is unfair to exclude their existence, though they are unhelpful for producing the line-emission).

The ‘standard’ and the dense clouds/filaments, coexisting in BLR, are likely to distribute in different regions. It is a consensus that the ‘standard’ clouds/filaments spread in the whole BLR, while a vast quantity of very dense cloudlets or filaments/sheets with small sizes are scattered in the very inner portion of BLR, most plausibly in the magnetosphere around the central engine—typically on scales of $d \lesssim 100 R_g$ ($R_g = GM/c^2$ is the gravitational radius of a central mass M), where the random magnetic fields of $10^3 - 10^4$ Gauss may pervade (Rees 1987; Ferland & Rees 1988; Guilbert & Rees 1988; Lightman & White 1988; Celotti et al. 1992; Sivron & Tsuruta 1993; Collin-Souffrin et al. 1996; Kuncic et al. 1996, 1997; Czerny & Dumont 1998; Celotti & Rees 1999; Lawrence 2012). The magnetic fields are likely to have complex structures. The dense cloudlets/filaments in the magnetosphere can be supported and confined by the magnetic fields. These dense cloudlets, with temperature of $\sim 10^4 - 10^5$ K, reprocess the primary non-thermal radiation of relativistic electrons from the central engine, and then contribute a quasi-blackbody continuum in the optical-UV bands (the ‘big blue bump’). A possible range of the density N_{H} and the size scale r for dense cloudlets/filaments/sheets were suggested by the above authors; $N_{\text{H}} \sim 10^{14} - 10^{18} \text{ cm}^{-3}$, $r \sim 10^2 - 10^9 \text{ cm}$ (for filaments and sheets, r expresses the thickness). Kuncic et al. (1996) further suggested that the most suitable values, favoring to surviving of the dense clouds around the central engine, are $N_{\text{H}} \sim 10^{16} - 10^{18} \text{ cm}^{-3}$ and $r \sim 10^2 - 10^6 \text{ cm}$. Besides, the presence of abundant fast electrons in the innermost region is conceivable. All these conditions are favorable to the production of the efficient Cerenkov line-like radiation. In brief, in our blend models, the dense cloudlets and the ‘standard’ cloudlets, respectively, exist in different regions of the BLR; the former are scattered in the inner magnetosphere around the central engine, whereas the latter distribute in the whole region of BLR. Some observations support the above picture of different regions: Bentz et al. (2010) reported that, the variation response of hydrogen lines to the UV-continuum in Arp 151 shows a deficit of prompt response in the Balmer-line cores but strong prompt response in the red wings of lines. This is easy to understand if the cores and the red-wings of lines are, respectively, dominated by the normal line and the Cerenkov line emissions; and if the latter is produced by the dense matter in the innermost region of BLR.

Moreover, we mention that, owing to the effect of the combined forces of gravity, radiation pressure and magnetic stresses, the dense clouds/filaments/sheets inside the magnetosphere should markedly deviate from the virial motion, controlled by the gravity alone, thus the speeds of clouds/filaments should be much less than the virial velocity due to the damping of both the radiation and the magnetic viscosity, i.e., $v \ll v_{\text{virial}} \approx v_{\text{ff}} = c(r/r_g)^{-1/2}$,

$r_g = GM/c^2$ is the gravitational radius with a central mass M . The possibility of $v < v_{\text{virial}}$ is confirmed by the observations: the observed broadening of the hydrogen lines, emitted simultaneously with the central flare, is markedly less than that given by the virial theorem (see the observed line widths in regions of time-delay $\tau \approx 0$ in Figures 3 and 4 in Bentz et al. (2010)). In the following calculations, we neglect both the velocity-broadening and velocity-shift of the Cerenkov lines, caused by the un-virial, slow flaring of dense clouds/filaments in the central magnetosphere. We assume that, all of the additional redshifts of hydrogen lines arise from the ‘Cerenkov line redshift’.

3. Redshifts of the pure Cerenkov Ly α , Ly β , H α , H β lines

Before the model calculations for the blended hydrogen lines, we first present the additional slight redshifts of pure Cerenkov hydrogen lines. For a specific Cerenkov quasi-line near the intrinsic wavelength $\lambda \gtrsim \lambda_{lu}$, the ‘Cerenkov line redshift’ is given by (You et al. 1984, 1986, 2000)

$$\Delta Z_{\lambda_{lu}}^{\text{Cer}} \equiv \frac{\Delta \lambda_p^{\text{Cer}}}{\lambda_{lu}} = 1.04 \times 10^{-11} \sqrt{\lambda_{lu} A_{ul} \Gamma_{lu} g_u \left(\frac{N_l}{g_l} - \frac{N_u}{g_u} \right) N_p^{-1} p^5} \quad (\text{valid for } N_{\text{H}} > 10^{15} \text{ cm}^{-3}). \quad (1)$$

Here, λ_{lu} is the intrinsic wavelength of a specific hydrogen line with the upper level u and lower level l ; A_{ul} is the Einstein’s spontaneous emission coefficient for the transition $u \rightarrow l$; $\Gamma_{lu} \equiv \Gamma_l + \Gamma_u = \sum_{i<l} A_{li} + \sum_{j<u} A_{uj}$ is the total quantum damping constant of the specific hydrogen line with wavelength λ_{lu} , which is related to Einstein’s spontaneous emission probabilities A_{li} and A_{uj} . g_u and g_l are the degeneracy of the upper level u and the lower level l , respectively. N_u and N_l represent, respectively, the number densities of neutral hydrogen at the upper and the lower levels. N_p is the number density of neutral hydrogen at the lowest level p of the photoelectric absorption, which gives the dominant absorption among all qualified photoelectric levels of a hydrogen atom for the incident line photon with wavelength λ_{lu} . For the Cerenkov Ly α and Ly β lines, $p = 2$; for the Cerenkov H α and H β lines, $p = 3$, etc. λ_{lu} is in unit cm.

From equation (1), we obtain the additional redshifts of the Cerenkov Ly α , Ly β , H α

and H β lines:

$$\begin{aligned}
 \Delta Z_{\text{Ly}\alpha}^{\text{Cer}} &= 1.93 \times 10^{-4} \left(\frac{N_1}{N_2} - \frac{1}{4} \right)^{1/2}, \\
 \Delta Z_{\text{Ly}\beta}^{\text{Cer}} &= 4.22 \times 10^{-5} \left(\frac{N_1}{N_2} - \frac{1}{9} \frac{N_3}{N_2} \right)^{1/2}, \\
 \Delta Z_{\text{H}\alpha}^{\text{Cer}} &= 3.13 \times 10^{-4} \left(\frac{N_2}{N_3} - \frac{4}{9} \right)^{1/2}, \\
 \Delta Z_{\text{H}\beta}^{\text{Cer}} &= 1.47 \times 10^{-4} \left(\frac{N_2}{N_3} - \frac{1}{4} \frac{N_4}{N_3} \right)^{1/2}, \tag{2}
 \end{aligned}$$

where N_1 , N_2 , N_3 and N_4 represent the number densities of neutral hydrogen in levels $n = 1, 2, 3$ and 4 , respectively. Here we adopt atomic parameters in Equation (1) as $\lambda_{12} = 1.216 \times 10^{-5}$ cm, $A_{21} = 4.70 \times 10^8$ s $^{-1}$, $\Gamma_{12} = A_{21}$, $\lambda_{13} = 1.026 \times 10^{-5}$ cm, $A_{31} = 5.57 \times 10^7$ s $^{-1}$, $\Gamma_{13} = 9.98 \times 10^7$ s $^{-1}$, $\lambda_{23} = 6.563 \times 10^{-5}$ cm, $A_{32} = 4.41 \times 10^7$ s $^{-1}$, $\Gamma_{23} = 5.70 \times 10^8$ s $^{-1}$, $\lambda_{24} = 4.861 \times 10^{-5}$ cm, $A_{42} = 8.42 \times 10^6$ s $^{-1}$, $\Gamma_{24} = 5.00 \times 10^8$ s $^{-1}$, $g_1 = 2$, $g_2 = 8$, $g_3 = 18$, and $g_4 = 32$ for our calculations.

We have mentioned that (Liu et al. 2014), the Cerenkov line-like radiation is effective only for the dense cloudlets (and/or filaments, sheets) with high densities $N_{\text{H}} \geq 10^{14}$ cm $^{-3}$. For the dense clouds, the populations of hydrogen, N_1 , N_2 , N_3 and N_4 , contained in Equation (2), are given by the Boltzmann law, thus $N_1/N_2 = (g_1/g_2) \exp(10.2 \text{ eV}/kT)$, $N_2/N_3 = (g_2/g_3) \exp(1.88 \text{ eV}/kT)$, and $N_4/N_3 = (g_4/g_3) \exp(-0.66 \text{ eV}/kT)$. Therefore the temperature T of the dense cloud/filament/sheet becomes an unique parameter for determining the ratios N_1/N_2 , N_2/N_3 and N_4/N_3 , hence for the redshifts $\Delta Z_{\text{Ly}\alpha}^{\text{Cer}}$, $\Delta Z_{\text{Ly}\beta}^{\text{Cer}}$, $\Delta Z_{\text{H}\alpha}^{\text{Cer}}$ and $\Delta Z_{\text{H}\beta}^{\text{Cer}}$ in Equation (2).

We obtain the permitted range of T of the dense matter in quasars as follows: As mentioned in Section 2, a vast amount of very dense and ‘cold’ clouds with typical temperature T of $\gtrsim 10^4$ K distribute in the magnetosphere around the central engine, which reprocess the non-thermal radiation from the central engine and contribute the ‘ultraviolet excess’ (the ‘big blue bump’) in the optical-ultraviolet continuum of quasars, via the optically thick thermal emission. This thermal component can be well described by a blackbody at a single temperature T . Malkan & Sargent (1982) successively fitted the observed spectra of ultraviolet excess of eight Seyfert 1 and quasars, and obtained the blackbody temperatures T in range 2×10^4 K $\lesssim T \lesssim 3 \times 10^4$ K (see Table 2 in Malkan & Sargent (1982)). The median or average temperature is $T \approx 2.5 \times 10^4$ K. They stressed that the thermal component need not be a single temperature blackbody. This is only the simplest form to fit the data well. In reality, there could be small contributions present from hotter or cooler gas which would be difficult to detect. Furthermore, the observation indicates that there is little thermal gas

much hotter than 40,000 K (Green et al. 1980). Therefore, in the following, we cease the calculations at $T = 4 \times 10^4$ K, and take 2×10^4 K $\lesssim T \lesssim 3 \times 10^4$ K as a permitted range of the temperature T .

By using equation (2), the calculated curves of Cerenkov line redshifts $\Delta Z_{\text{Ly}\alpha}^{\text{Cer}} \sim T$, $\Delta Z_{\text{Ly}\beta}^{\text{Cer}} \sim T$, $\Delta Z_{\text{H}\alpha}^{\text{Cer}} \sim T$ and $\Delta Z_{\text{H}\beta}^{\text{Cer}} \sim T$, are shown in Figure 1 by the solid, dashed, dotted and dash-dotted lines respectively, taking the temperature T of the dense clouds/filaments/sheets in quasars as a free variable. In Figure 1, the permitted range of T is labeled by the vertical dash-dot-dotted lines. In this region, the calculated Cerenkov redshifts are restricted in ranges $6.88 \times 10^{-4} \lesssim \Delta Z_{\text{Ly}\alpha}^{\text{Cer}} \lesssim 1.86 \times 10^{-3}$, $1.51 \times 10^{-4} \lesssim \Delta Z_{\text{Ly}\beta}^{\text{Cer}} \lesssim 4.07 \times 10^{-4}$, $2.15 \times 10^{-4} \lesssim \Delta Z_{\text{H}\alpha}^{\text{Cer}} \lesssim 2.93 \times 10^{-4}$, and $1.11 \times 10^{-4} \lesssim \Delta Z_{\text{H}\beta}^{\text{Cer}} \lesssim 1.48 \times 10^{-4}$, respectively.

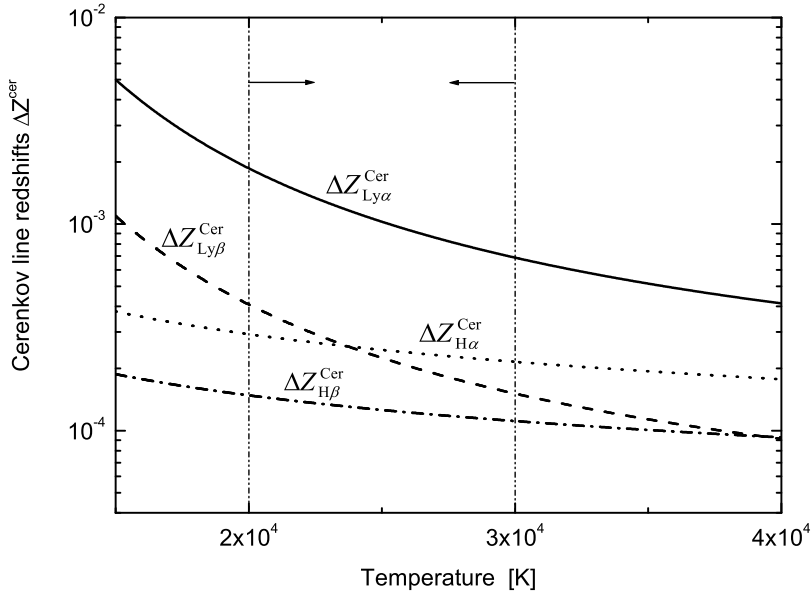


Fig. 1.— The calculated redshifts of Cerenkov Ly α , Ly β , H α and H β lines under different temperature of the dense clouds in quasars, shown by the solid, dashed, dotted and dash-dotted lines, respectively. The vertical dash-dot-dotted lines label the permitted temperature range of dense matter, 2×10^4 K $\lesssim T \lesssim 3 \times 10^4$ K, which is obtained by fitting the ‘big blue bump’ in the observed optical-UV continua of quasars (Malkan & Sargent 1982) .

We mention that, actually, the observed $\Delta Z_{\text{Ly}\alpha}^{\text{obs}}$, $\Delta Z_{\text{H}\alpha}^{\text{obs}}$ and $\Delta Z_{\text{H}\beta}^{\text{obs}}$, listed in Table 1, are the averaged values of $\sim 2,200$ quasars (Vanden Berk et al. 2001). Therefore it is more reasonable to make a theoretical calculation of redshifts at the average temperature T , and then to compare with the average observed ones. Taking the median temperature

$T \approx 2.5 \times 10^4$ K ($kT \approx 2.2$ eV) in range 2×10^4 K $\lesssim T \lesssim 3 \times 10^4$ K, the corresponding median values of redshifts $\Delta Z_{\text{Ly}\alpha}^{\text{Cer}}$, $\Delta Z_{\text{Ly}\beta}^{\text{Cer}}$, $\Delta Z_{\text{H}\alpha}^{\text{Cer}}$ and $\Delta Z_{\text{H}\beta}^{\text{Cer}}$ are listed in the second line in Table 1.

Table 1: Observed and theoretically calculated values of the additional slight redshifts of Ly α , Ly β , H α , H β lines relative to [O III] 5007 Å

	Ly α	Ly β	H α	H β
Observed mean	$\Delta Z_{\text{Ly}\alpha}^{\text{obs}}(10^{-4})$	$\Delta Z_{\text{Ly}\beta}^{\text{obs}}(10^{-4})$	$\Delta Z_{\text{H}\alpha}^{\text{obs}}(10^{-4})$	$\Delta Z_{\text{H}\beta}^{\text{obs}}(10^{-4})$
redshift values ¹	(4.77 ± 3.03)	—	(0.93 ± 0.43)	(0 ± 0.50)
Redshifts of Cerenkov	$\Delta Z_{\text{Ly}\alpha}^{\text{Cer}}(10^{-4})$	$\Delta Z_{\text{Ly}\beta}^{\text{Cer}}(10^{-4})$	$\Delta Z_{\text{H}\alpha}^{\text{Cer}}(10^{-4})$	$\Delta Z_{\text{H}\beta}^{\text{Cer}}(10^{-4})$
hydrogen lines ²	9.77	2.14	2.42	1.24
Expected redshifts of	$\Delta Z_{\text{Ly}\alpha}^{\text{Exp}}(10^{-4})$	$\Delta Z_{\text{Ly}\alpha}^{\text{Exp}}(10^{-4})$	$\Delta Z_{\text{H}\alpha}^{\text{Exp}}(10^{-4})$	$\Delta Z_{\text{H}\beta}^{\text{Exp}}(10^{-4})$
the blended hydrogen	4.88	1.07	1.21	0.62
lines ³ (blend model 1)				
Expected redshifts of	$\Delta Z_{\text{Ly}\alpha}^{\text{Exp}}(10^{-4})$	$\Delta Z_{\text{Ly}\alpha}^{\text{Exp}}(10^{-4})$	$\Delta Z_{\text{H}\alpha}^{\text{Exp}}(10^{-4})$	$\Delta Z_{\text{H}\beta}^{\text{Exp}}(10^{-4})$
the blended hydrogen	4.76	—	0.94	0
lines ⁴ (blend model 2)				

Notes. — 1. The observation data are taken from Table 4 in Vanden Berk et al. (2001) with a large data set of over 2200 quasars. 2. In this calculation, we take a median temperature $T \approx 2.5 \times 10^4$ K (or $kT \approx 2.2$ eV) in the permitted temperature range of dense clouds, 2×10^4 K $\lesssim T \lesssim 3 \times 10^4$ K (Malkan & Sargent 1982, for calculation details see Section 3). 3. For the blend model 1, we adopt a simple equipartition of intensity between the normal line and the Cerenkov line, $I_{\lambda_{lu}}^{\text{nor}} \approx I_{\lambda_{lu}}^{\text{Cer}}$ (for details, see Section 4). 4. For the blended model 2, we take the intensity-ratio $I_{\text{Ly}\alpha}^{\text{Cer}}/I_{\text{Ly}\alpha}^{\text{nor}} = 0.95$, $I_{\text{H}\alpha}^{\text{Cer}}/I_{\text{H}\alpha}^{\text{nor}} = 0.63$ and $I_{\text{H}\beta}^{\text{Cer}}/I_{\text{H}\beta}^{\text{nor}} = 0$, to get the best fitting with the observed redshifts values.

We notice that, the above calculated redshifts of the pure Cerenkov lines, listed in the second line of Table 1, are already comparable with the observed values, with the same orders of magnitude of $\Delta Z \approx 10^{-4}$ and same un-equality sequence $\Delta Z_{\text{Ly}\alpha} > \Delta Z_{\text{H}\alpha} > \Delta Z_{\text{H}\beta}$. This is unlikely a coincidence, though the discrepancy between the theoretical and the observational values can not be ignored.

4. Model calculation of redshifts of the blended hydrogen lines

Table 1 shows a marked deviation of the redshifts of pure Cerenkov hydrogen Ly α , H α and H β lines from the observed values, though with the same order of magnitude $\Delta Z \sim 10^{-4}$. The theoretical redshifts are higher than the corresponding observed ones, $\Delta Z_{\text{Ly}\alpha}^{\text{Cer}} > \Delta Z_{\text{Ly}\alpha}^{\text{obs}}$, $\Delta Z_{\text{H}\alpha}^{\text{Cer}} > \Delta Z_{\text{H}\alpha}^{\text{obs}}$ and $\Delta Z_{\text{H}\beta}^{\text{Cer}} > \Delta Z_{\text{H}\beta}^{\text{obs}}$. This is easy to understand in the frame of the ‘blend models’. As a blended line, the observed broad hydrogen line contains another important component—the ‘normal line’, which has not been taken into account yet (note that, in the composite spectra of Vanden Berk et al. (2001), both the broad and the narrow ‘normal lines’ (the bound-bound transition lines) are all involved in the observed broad hydrogen lines). Differing to the Cerenkov component, the ‘normal line’ exactly locates at $\lambda = \lambda_{lu}$, with no additional redshift ($\Delta Z_{\lambda_{lu}}^{\text{nor}} = 0$), which inevitably leads to a marked decrease of the resultant redshift of the ‘blended line’.

The expected redshift of a blended line is determined by the fraction of the Cerenkov component in the total line intensity,

$$\begin{aligned} \Delta Z_{\lambda_{lu}}^{\text{exp}} &= \left(\frac{1}{I_{\lambda_{lu}}^{\text{nor}} + I_{\lambda_{lu}}^{\text{Cer}}} \right) (I_{\lambda_{lu}}^{\text{nor}} \Delta Z_{\lambda_{lu}}^{\text{nor}} + I_{\lambda_{lu}}^{\text{Cer}} \Delta Z_{\lambda_{lu}}^{\text{Cer}}) \\ &= \left(\frac{I_{\lambda_{lu}}^{\text{Cer}}}{I_{\lambda_{lu}}^{\text{nor}} + I_{\lambda_{lu}}^{\text{Cer}}} \right) \Delta Z_{\lambda_{lu}}^{\text{Cer}} \quad (\text{where } \Delta Z_{\lambda_{lu}}^{\text{nor}} = 0), \end{aligned}$$

or

$$\Delta Z_{\lambda_{lu}}^{\text{exp}} = \left(\frac{I_{\lambda_{lu}}^{\text{Cer}} / I_{\lambda_{lu}}^{\text{nor}}}{1 + I_{\lambda_{lu}}^{\text{Cer}} / I_{\lambda_{lu}}^{\text{nor}}} \right) \Delta Z_{\lambda_{lu}}^{\text{Cer}}. \quad (3)$$

where $I_{\lambda_{lu}}^{\text{Cer}}$ and $I_{\lambda_{lu}}^{\text{nor}}$ are the line-intensities of the Cerenkov quasi-line and the normal line, respectively. The total intensity of the blend line is $I_{\lambda_{lu}}^{\text{total}} = I_{\lambda_{lu}}^{\text{nor}} + I_{\lambda_{lu}}^{\text{Cer}}$. Equation (3) is a good approximation for describing the resultant redshift of a blended line, where the peak of the Cerenkov line quasi-line is very closed to the accompanying normal line.

In order to obtain the expected redshift of a blended line, it is necessary to know the intensity-ratio $I_{\lambda_{lu}}^{\text{Cer}} / I_{\lambda_{lu}}^{\text{nor}}$ of the two components. This could be a tedious work, depending on a detailed data-analysis for both the observed intensities and the redshifts of different hydrogen lines of quasars. We plan to do it in near future. In this paper, we tentatively take the intensity-ratio in Equation (3) as a modulated parameter to calculate $\Delta Z_{\lambda_{lu}}^{\text{exp}}$, and then to compare with observations. We envisage the values of intensity-ratio $I_{\lambda_{lu}}^{\text{Cer}} / I_{\lambda_{lu}}^{\text{nor}}$ in two manners, which we call as the ‘blend model 1’ and the ‘blend model 2’ in the following, respectively.

4.1. Blend model 1

As a primary approximation, we simply assume that, the average intensity-ratio in the blend line of quasars is near to unit,

$$I_{\lambda_{lu}}^{\text{Cer}}/I_{\lambda_{lu}}^{\text{nor}} \approx 1, \quad (4)$$

i.e., we have an ‘equipartition of intensity’ between the two components in the blend lines. Although so far we can not give a convincing argument to show the reasonableness of the approximate Equation (4), but we have emphasized the importance of the Cerenkov component in quasars. We mentioned that the Cerenkov quasi-line is strong enough to compete with the accompanying normal line in the blended hydrogen lines or low-ionization lines (Liu et al. 2014). This implies that the intensity-ratio of the Cerenkov quasi-line to the normal line should be not far from unit, e.g., in a narrower range $0.5 < I_{\lambda_{lu}}^{\text{Cer}}/I_{\lambda_{lu}}^{\text{nor}} < 1.5$. Therefore, in the primary $\Delta Z_{\lambda_{lu}}^{\text{exp}}$ -calculations, the approximate Equation 4, $I_{\lambda_{lu}}^{\text{Cer}} \approx I_{\lambda_{lu}}^{\text{nor}}$, seems to be acceptable. Inserting Equation (4) into Equation (3), we obtain

$$\Delta Z_{\lambda_{lu}}^{\text{exp}} \approx \frac{1}{2} \Delta Z_{\lambda_{lu}}^{\text{Cer}} \quad (\text{when } I_{\lambda_{lu}}^{\text{Cer}}/I_{\lambda_{lu}}^{\text{nor}} \approx 1) \quad (5)$$

By using Equation (5), the expected resultant redshifts of the blended hydrogen lines $\text{Ly}\alpha$, $\text{Ly}\beta$, $\text{H}\alpha$ and $\text{H}\beta$ are shown in the third line in Table 1. Obviously, the expected redshifts, given by the ‘blend model 1’, are much closer to the observed ones (Table 1, the first line), than the pure Cerenkov lines (the second line in Table 1). This result strongly supports the reasonableness of our proposition of the blended hydrogen lines.

However, there still exist remarkable discrepancies between the predictions of model 1 and the observations for the $\text{H}\alpha$ and $\text{H}\beta$ lines (particularly for $\text{H}\beta$), indicating that the approximation of ‘equipartition of intensity’ (Equations (4) and (5)) is not equally good for all hydrogen lines. This is easy to understand. In fact, the Cerenkov and the normal line emissions are in principle different mechanisms, independent to each other. Generally, the series of intensity-ratios of the Cerenkov hydrogen lines, $I_{\text{Ly}\alpha}^{\text{Cer}}/I_{\text{Ly}\beta}^{\text{Cer}}/I_{\text{H}\alpha}^{\text{Cer}}/I_{\text{H}\beta}^{\text{Cer}}$ should be different to $I_{\text{Ly}\alpha}^{\text{nor}}/I_{\text{Ly}\beta}^{\text{nor}}/I_{\text{H}\alpha}^{\text{nor}}/I_{\text{H}\beta}^{\text{nor}}$ for the normal lines. Therefore, $I_{\text{Ly}\beta}^{\text{Cer}} \neq I_{\text{Ly}\beta}^{\text{nor}}$, $I_{\text{H}\alpha}^{\text{Cer}} \neq I_{\text{H}\alpha}^{\text{nor}}$, and $I_{\text{H}\beta}^{\text{Cer}} \neq I_{\text{H}\beta}^{\text{nor}}$, etc. even if $I_{\text{Ly}\alpha}^{\text{Cer}} = I_{\text{Ly}\alpha}^{\text{nor}}$ is already given.

4.2. Blend model 2

In this model, we abandon Equations (4) and (5), tentatively take the line-intensity ratio $I_{\lambda_{lu}}^{\text{Cer}}/I_{\lambda_{lu}}^{\text{nor}}$ in Equation (3) as a modulated parameter to get the best fitting to each

observed redshifts for Ly α , H α and H β lines. Taking $I_{\text{Ly}\alpha}^{\text{Cer}}/I_{\text{Ly}\alpha}^{\text{nor}} = 0.95$, $I_{\text{H}\alpha}^{\text{Cer}}/I_{\text{H}\alpha}^{\text{nor}} = 0.63$, $I_{\text{H}\beta}^{\text{Cer}}/I_{\text{H}\beta}^{\text{nor}} = 0$, from Equation (3), we obtain the best expected redshifts of Ly α , H α and H β lines, shown in the fourth line in Table 1, which are in good consistence with the observed values. The good fitting shows the plausibility of above adopted intensity-ratios in quasars, though the theoretical argument has not been given yet.

But we would like to mention that, the chosen value $I_{\text{H}\beta}^{\text{Cer}}/I_{\text{H}\beta}^{\text{nor}} = 0$ for fitting the ‘zero redshift’ of H β line seems to be quite questionable. The observed $\Delta Z_{\text{H}\beta}^{\text{obs}} = (0 \pm 0.50) \times 10^{-4}$, with the largest error of measurement among Ly α , H α and H β lines, only indicates that no additional redshift can be detected at the level of order of magnitude $\Delta Z \sim 10^{-4}$; and the observed redshift is uncertain in a wide range, $0 \leq \Delta Z_{\text{H}\beta}^{\text{obs}} \leq 0.5 \times 10^{-4}$, rather than $\Delta Z_{\text{H}\beta}^{\text{obs}} = 0$. Correspondingly, the ratio $I_{\text{H}\beta}^{\text{Cer}}/I_{\text{H}\beta}^{\text{nor}}$ should be taken in a wider range, $I_{\text{H}\beta}^{\text{Cer}}/I_{\text{H}\beta}^{\text{nor}} \leq 0.5$, rather than $I_{\text{H}\beta}^{\text{Cer}}/I_{\text{H}\beta}^{\text{nor}} = 0$. Anyway, the following conclusion remains beyond doubt: the ratio $I_{\text{H}\beta}^{\text{Cer}}/I_{\text{H}\beta}^{\text{nor}}$ for the blend H β line should be far from the ‘equipartition of intensity’. The small values of $I_{\text{H}\beta}^{\text{Cer}}/I_{\text{H}\beta}^{\text{nor}}$ (in range $I_{\text{H}\beta}^{\text{Cer}}/I_{\text{H}\beta}^{\text{nor}} \leq 0.5$) imply that, comparing with Ly α and H α lines, the Cerenkov component in the blend H β line is no longer important, rendering the ‘Cerenkov line redshift’ difficult to be detected (see Equation (3), and the first line in Table 1).

5. Conclusions and Discussions

Table 1 shows that, the expected redshifts of the blended hydrogen lines, given by model 1 or 2, are well fitted to the observed values. Furthermore, comparing the observations and the predictions of model 1 or model 2 (see the first, third and fourth lines in Table 1), we find that, both the observed and the predicted redshifts have the same un-equality sequence, i.e., $\Delta Z_{\text{Ly}\alpha}^{\text{obs}} > \Delta Z_{\text{H}\alpha}^{\text{obs}} > \Delta Z_{\text{H}\beta}^{\text{obs}}$, as well as $\Delta Z_{\text{Ly}\alpha}^{\text{exp}} > \Delta Z_{\text{H}\alpha}^{\text{exp}} > \Delta Z_{\text{H}\beta}^{\text{exp}}$. We stress that this un-equality sequence originates from the intrinsic property of the Cerenkov hydrogen lines, $\Delta Z_{\text{Ly}\alpha}^{\text{Cer}} > \Delta Z_{\text{H}\alpha}^{\text{Cer}} > \Delta Z_{\text{H}\beta}^{\text{Cer}}$, despite what T -value is adopted (see Figure 1). We claim that, the good consistency, and the same un-equality sequence between observations and predictions, are not coincident, instead, it is an important evidence supporting the conclusion: the observed hydrogen lines of quasars are blended by both the Cerenkov quasi-line and the normal line; and the redshift-differences of different hydrogen lines originate from the ‘Cerenkov line redshifts’, existing in the blended lines.

Another conclusion is that the average intensity ratios of the two components in the blended hydrogen lines of $\sim 2,200$ quasars are not far from unit (approximate ‘equipartition of intensity’). We particularly conclude that, for the strongest Ly α line, $I_{\text{Ly}\alpha}^{\text{Cer}}/I_{\text{Ly}\alpha}^{\text{nor}} \approx 1$ is more reliable because of the good fitting to the observed Ly α line (both in the blend model

1 and model 2, a more exact value should be $I_{Ly\alpha}^{Cer}/I_{Ly\alpha}^{nor} \approx 0.95$, given by blend model 2). This could be a progress in study of the blend models for the broad lines of quasars; the ‘equipartition of intensity’ for Ly α line, the strongest one in all hydrogen lines, numerically confirms the importance of the Cerenkov line-like radiation for the broad lines of quasars, which can not be ignored any more.

The ratios $I_{Ly\alpha}^{Cer}/I_{Ly\alpha}^{nor} = 0.95$, $I_{H\alpha}^{Cer}/I_{H\alpha}^{nor} = 0.63$, and $I_{H\beta}^{Cer}/I_{H\beta}^{nor} \leq 0.5$, adopted in the model 2, could be also helpful to estimate the intensity-ratios of different blended hydrogen lines, $I_{Ly\alpha}^{exp}/I_{H\alpha}^{exp}/I_{H\beta}^{exp}$, where $I_{Ly\alpha}^{exp} \equiv I_{Ly\alpha}^{Cer} + I_{Ly\alpha}^{nor}$ represents the total intensity of the blend Ly α line, similarly for $I_{H\alpha}^{exp}$, $I_{H\beta}^{exp}$. If the above parameter-values $I_{Ly\alpha}^{Cer}/I_{Ly\alpha}^{nor} = 0.95$, $I_{H\alpha}^{Cer}/I_{H\alpha}^{nor} = 0.63$, and $I_{H\beta}^{Cer}/I_{H\beta}^{nor} \leq 0.5$ (model 2) also give a good fitting to the observed intensity-ratios $I_{Ly\alpha}^{obs}/I_{H\alpha}^{obs}/I_{H\beta}^{obs}$, the proposition of blended broad lines in quasars would be further confirmed. This is worth to do in subsequent study.

The observed additional redshifts of the low-ionization lines, relative to [O III] 5007 Å (e.g., Mg II 2798 Å, see Table 4 in Vanden Berk et al. (2001)), should be also arise from the ‘Cerenkov line redshift’, because the low-ionization lines also contain the Cerenkov quasi-line component. We plan to fit the redshifts of some low-ionization lines in the same way as for the hydrogen lines, taking the intensity-ratios (e.g., $I_{MgII}^{Cer}/I_{MgII}^{nor}$) as parameters.

In our blend model consideration, the ‘Cerenkov line shift’ is the unique source of the additional redshifts of hydrogen lines. Therefore, the ‘blend models 1 and 2’ are basically different from the generally accepted ‘stratification models’, in which the additional redshifts all arise from the Doppler effect (the velocity shift). The advantage of the ‘blend models’ is obvious, which gives the best fitting to the observed redshifts. We hope that the future observations can give a further judgment on the two different kinds of models.

As of now there remain some outstanding difficulties in the current standard models to account for the observed broad hydrogen lines and some low-ionization lines in quasars, such as the steep Balmer decrement (e.g., Osterbrock 1984; Kwan & Krolik 1979, 1981; Drake & Ulrich 1980; Korista & Goad 2004), the different redshift values among some broad lines, the excess line emission (i.e., the energy-budget discrepancy of Fe II, Mg II, He II lines in UV and optical wavebands, Netzer 1985; Collin-Souffrin 1986; MacAlpine 2003; Baldwin et al. 2004; Joly et al. 2008). The quasi-line emission could provide a solution for these long standing puzzles, for which the energy is extracted from the kinetic energy of the fast electrons, rather than from the continuum photons. We hope that the existence of the component of this quasi-line emission in broad lines of quasars can be tested by future observations.

The shape and redshift of emission lines in quasars reveal the physical processes and

activities of central engine around black hole. Until now, Gaskell’s results on the difference between low- and high-ionization lines (represented by Mg II (2800 Å) and C IV (1549 Å) respectively) have remained valid, and have yielded the observational basis for a model that still provides a basic interpretative sketch for the structure of broad line emitting region (Collin-Souffrin et al. 1988). In their model, the low-ionization lines(LILs) and the hydrogen lines of quasars have a systemic redshift relative to the high-ionization lines(HILs) (Gaskell 1982; Wilkes 1986; Corbin 1990, 1991; Espey et al. 1989; Carswell et al. 1991; Sulentic et al. 1995; McIntosh et al. 1999). They think that HIL blue shifts are associated with radial motion in a flattened structure (e.g., the accretion disk) mainly emitting LILs, also later developments confirmed the earlier results (Corbin & Boroson 1996; Marziani et al. 1996). However, Sulentic et al. (2016) pointed out that not all quasars are the same case, and that a first distinction between radio-loud and radio-quiet quasars was necessary: blueshifts were mostly present in radio quiet (RQ) quasars, but definitely rarer in radio loud (RL) (also see, Sulentic et al. 2000, 2007). We explain redshifts between the HILs and the LILs based on our primary idea, which the HILs are mainly from the normal lines (i.e., bound-bound transition), whereas the LILs are blended by the component of Cerenkov quasi-line, which has an intrinsic redshift from line to line. Besides, this thought should be expected to be confirmed that the Cerenkov quasi-line emission has much more contribution to broad lines in RQ quasars because there may be much denser gas ($N_{\text{H}} \geq 10^{14} \text{ cm}^{-3}$) required by Cerenkov emission.

We would like to thank the anonymous referee for his/her careful reading of our manuscript which would help us to improve it. DL acknowledges support by the National Science Foundation of China (Grant Nos. 11078014 and 11125313), the key laboratory grant from the Office of Science and Technology, Shanghai Municipal Government (No. 11DZ2260700), the National Basic Research Program of China (Grant Nos. 2009CB824904 and 2013CB837901), and the Shanghai Science and Technology Commission (Program of Shanghai Subject Chief Scientist; Grant Nos. 12XD1406200 and 11DZ2260700).

REFERENCES

- Baldwin, J. A., Ferland, G. J., Korista, K. T., Hamann, F., & La Cluyze, A., 2004, *ApJ*, 615, 610
- Bentz, M. C., Horne, K., Barth, A. J., et al. 2010, *ApJ*, 720, L46
- Carswell, R. F., Mountain, C. M., Robertson, D. J., Beard, S. M., Glendinning, A. R., Laird, D. C., Lawrence, L. C., Montgomery, D., Pentland, G., Pickup, D. A., Smith, I. A.,

- Bailey, J. A., Bridger, A., Casali, M. M., Geballe, T. R., Puxley, P., Smith, M. G., Wright, G. S., Ramsay, S. K., Baker, A. C., Espey, B. R., & Ward, M. J. 1991, *ApJ*, 381, L5
- Catravas, P., Chattopadhyay, S., Esarey, E., Leemans, W. P., Assmann, R., Decker, F. J., Hogan, M. J., Iverson, R., Siemann, R. H., Walz, D., Whittum, D., Blue, B., Clayton, C., Joshi, C., Marsh, K. A., Mori, W. B., Wang, S., Katsouleas, T., Lee, S., & Muggli, P., 2001, *Physical Review E*, 64, 046502
- Celotti, A., Fabian, A. C., & Rees, M. J. 1992, *MNRAS*, 255, 419
- Celotti, A. & Rees, M. J. 1999, *MNRAS*, 305, L41
- Chen, L., You, J. H., & Liu, D. B. 2005, *ApJ*, 627, 177
- Cheng, F. H., You, J. H., & Yan, M. 1990, *ApJ*, 358, 18
- Collin-Souffrin, S. 1986, *A&A*, 166, 115
- Collin-Souffrin, S., Dyson, J. E., McDowell, A. M., & Zycki, J. J. 1988, *MNRAS*, 232, 539
- Collin-Souffrin, S., Czerny, B., Dumond, A. M., & Zycki, P. T. 1996, *A&A*, 314, 393
- Corbin, M. R. 1990, *ApJ*, 350, 346
- Corbin, M. R. 1991, *ApJ*, 371, L51
- Corbin, M. R. & Boroson, T. A. 1996, *ApJS*, 107, 69
- Czerny, B., & Dumont, A. M. 1998, *A&A*, 338, 386
- Davidson, K., & Netzer, H. 1979, *Rev. Mod. Phys.*, 51, 715
- (Drake), S. A., & Ulrich, R. K., 1980, *ApJS*, 42, 351
- Espey, B. R., Carswell, R. F., Bailey, J. A., Smith, M. G., & Ward, M. J. 1989, *ApJ*, 342, 666
- Ferland, G. J. & Rees, M. J. 1988, *ApJ*, 332, 141
- Gaskell, C. M. 1982, *ApJ*, 263, 79
- Gaskell, C. M. & Goosmann, R. W. 2013, *ApJ*, 769, 30
- Green, R. F., Pier, J. R., Schmidt, M., Estabrook, F. B., Lane, A., & Wahlquist, H. D. 1980, *ApJ*, 239, 483

- Guilbert, P. W. & Rees, M. J. 1988, *MNRAS*, 233, 475
- Halenka, J., Olchawa, W., Madej, J., & Grabowski, B. 2015, *ApJ*, 808, 131
- Halpern, J. P. & Eracleous, M. 2000, *ApJ*, 531, 647
- Ji, T., Wang, T. G., Zhou, H. Y., & Wang, H. Y., 2012, *Research in Astronomy and Astrophysics*, 12, 369
- Joly, M., Veron-Cetty, M., Veron, P. 2008, *RMxAC*, 32, 59
- Koratkar, A. P. & Gaskell, C. M. 1991, *ApJS*, 75, 719
- Korista, K. T. 1992, *ApJS*, 79, 285
- Korista, K. T. & Goad, M. R. 2004, *ApJ*, 606, 949
- Kuncic, Z., Blackman, E. G., & Rees, M. J. 1996, *MNRAS*, 283, 1322
- Kuncic, Z., Celloti, A., & Rees, M. J. 1997, *MNRAS*, 284, 717
- Kwan, J. & Krolik, J. H., 1979, *ApJ*, 233, L91
- Kwan, J. & Krolik, J. H., 1981, *ApJ*, 250, 478
- Lawrence, A. 2012, *MNRAS*, 423, 451
- Laor, A. 2006, *ApJ*, 643, 112
- Lightman, A. P., & White, T. R. 1988, *ApJ*, 335, 57
- Liu, D. B., Chen, W. P., You, J. H., & Chen, L. 2014, *ApJ*, 780, 89
- MacAlpine, G. M. 2003, *RMxAC*, 18, 63
- Malkan, M. A. & Sargent, W. L. 1982, *ApJ*, 254, 22
- Marziani, P., Sulentic, J. W., Dultzin-Hacyan, D., Calvani, M., & Moles, M., 1996, *ApJS*, 104, 37
- McIntosh, D. H., Rix, H. W., Rieke, M. J., & Foltz, C. B. 1999, *ApJ*, 517, L73
- Netzer, H. 1977, *MNRAS*, 181, 89
- Netzer, H. 1985, *ApJ*, 289, 451

- Nishihara, E., Yamashita, T., Yoshida, M., Watanabe, E., Okumura, S. I., Mori, A., & Iye, M. 1997, *ApJ*, 488, L27
- Osterbrock, D. E., 1979, *Publ. Astron. Soc. Pac.*, 91, 608
- Osterbrock, D. E., 1984, *QJRAS*, 25, 1
- Osterbrock, D. E., & Ferland, G. J. 2006, *Astrophysics of Gaseous Nebulae and Active Galactic Nuclei* (California: University Science Books)
- Peterson, B. M., & Wandel, A., 1999, *ApJ*, 521, L95
- Rees, M. J., 1987, *MNRAS*, 228, 47
- Rees, M. J., Netzer, H., & Ferland, G. J. 1989, *ApJ*, 347, 640
- Shadmehri, M., 2015, *MNRAS*, 451, 3671
- Smith, J. E., Robinson, A., Young, S, Axon, D. J., & Corbett, E. A. 2005, *MNRAS*, 359, 846
- Sivron, R.& Tsuruta, S. 1993, *ApJ*, 402, 420
- Sulentic, J. W., Marziani, P., Dultzin-Hacyan, D., Calvani, M., & Moles, M. 1995, *ApJ*, 445, L85
- Sulentic, J. W., Marziani, P., & Dultzin-Hacyan, D. 2000, *ARA&A*, 38, 521
- Sulentic, J. W., Bachev, R., Marziani, P., Negrete, C. A., & Dultzin, D. 2007, *ApJ*, 666, 757
- Sulentic, J. W., Marziani, P., Del Olmo, A., & Zamfir, S. 2016, *Ap&SS*, 361, 55
- Vanden Berk, D. E., Richards, G. T., & Bauer, B., et al. 2001, *AJ*, 122, 549
- Wilkes, B. J. 1986, *MNRAS*, 218, 331
- Xu, K. Z., Yang, B. X., Xi, F. Y., Wu, W. M., & Hao, L. Y., 1988, *Physical Review A*, 37, 2912
- Yang, B. X., Xu, K. Z., Hao, L. Y. & Xu, X. L., 1989, *Physical Review A*, 40, 5411
- You, J. H., Kiang, T., Cheng, F. Z., & Cheng, F. H. 1984, *MNRAS*, 780, 89
- You, J. H., Cheng, F. H., Cheng, F. Z., & Kiang, T. 1986, *Phy. Rev. A*, 34, 3015
- You, J. H., Xu, Y. D., Liu, D. B., Shi, J. R., & Jin, G. X. 2000, *A&A*, 362, 762

